Towards a sector-specific CO/CO$_2$ emission ratio: Satellite-based observation of CO release from steel production in Germany

Oliver Schneising, Michael Buchwitz, Maximilian Reuter, Michael Weimer, Heinrich Bovensmann, John P. Burrows, and Hartmut Bösch

Institute of Environmental Physics (IUP), University of Bremen FB1, Bremen, Germany

Correspondence: O. Schneising (oliver.schneising@iup.physik.uni-bremen.de)

Abstract.

Global crude steel production is expected to continue to increase in the coming decades to meet the demands of the growing world population. Currently, the dominant steelmaking technology worldwide is the conventional highly CO$_2$-intensive Blast Furnace–Basic Oxygen Furnace production route (also known as the Linz–Donawitz process) using iron ore as raw material and coke as a reducing agent. As a result, large quantities of special gases that are rich in carbon monoxide (CO) are by-products of the various stages of the steelmaking process. Given the challenges associated with satellite-based estimates of carbon dioxide (CO$_2$) emissions at the scale of emitting installations due to significant background levels, co-emitted CO may serve as a valuable indicator of the carbon footprint of steel plants.

We show that regional CO release from steel production sites can be monitored from space using 5 years of measurements (2018-2022) from the TROPOspheric monitoring instrument (TROPOMI) on board the Sentinel-5 Precursor satellite benefiting from its relatively high spatial resolution and daily global coverage. We analyse all German steel plants with blast furnaces and basic oxygen furnaces and obtain associated CO emissions in the range of 50-400 $\mathrm{kt\,yr^{-1}}$ per site. A comparison with the respective CO$_2$ emissions on the level of emitting installations available from emissions trading data of the European Union Emissions Trading System yields a linear relationship with a sector-specific CO/CO$_2$ emission ratio for the analysed steelworks of $3.24\%\,[2.73-3.89;\,1\sigma]$ suggesting the feasibility of using CO as a proxy for CO$_2$ emissions from comparable steel production sites.

1 Introduction

Carbon monoxide (CO) has a dual role as both an air pollutant and a crucial component of atmospheric chemistry. Its reactivity with the hydroxyl radical (OH) and other atmospheric constituents has a significant effect on the oxidising capacity of the atmosphere, which subsequently influences the abundances of greenhouse gases, such as methane, and the formation of secondary pollutants, including tropospheric ozone (Holloway et al., 2000). It is therefore essential to gain accurate knowledge of the sources of CO to ensure efficient air quality control, pollution management, and an improved understanding of atmospheric composition and its impact on climate change. The atmospheric lifetime of CO is approximately 1-2 months, so that it is well suited for tracing the transport of pollutants and can be used as a proxy for co-emitted CO$_2$ (Wu et al., 2022; MacDonald et al.,

25 2023), which is harder to observe from space than CO because CO_2 is well-mixed in the atmosphere resulting in small signals relative to large background levels.

Satellite missions with global coverage significantly improve our ability to analyse atmospheric CO. Instruments using measurements of shortwave infrared (SWIR) radiances to retrieve CO column abundances in the atmosphere are sensitive to the planetary boundary layer and operate during daytime when there is sufficient sunlight to illuminate the Earth's surface.

30 Prominent instruments measuring in this spectral range include the Measurement of Pollution in the Troposphere (MOPITT) instrument (Drummond et al., 2010) on board NASA's Terra satellite, the SCanning Imaging Absorption spectroMeter for Atmospheric CHartographY (SCIAMACHY) (Burrows et al., 1995; Bovensmann et al., 1999) on board ESA's ENVISAT, and the Thermal And Near infrared Sensor for carbon Observations Fourier Transform Spectrometer 2 (TANSO-FTS-2) on board GOSAT-2 (Suto et al., 2021). The application areas for satellite data were further extended with the TROPOspheric Moni-

35 toring Instrument (TROPOMI) (Veefkind et al., 2012), which is considered a milestone for the determination of atmospheric composition, including CO, from space by combining high spatio-temporal sampling and data quality.

Major sources of CO emissions include transportation, residential heating and cooking, biomass burning, industrial processes, and natural sources like wildfires. In the broader category of industrial emissions, CO is generated as a byproduct of incomplete combustion or chemical reactions. An important example is the steel producing industry with CO emissions

40 mainly due to the formation and release of CO-rich gases in the widely used Linz–Donawitz process of integrated steel plants: 1) Sinter gas produced in a pre-treatment process step agglomerating iron ore fines into a porous, consistent high quality burden suitable for direct use in the blast furnace, 2) blast furnace gas arising during iron ore reduction with carbon (primarily in the form of coke), and 3) converter gas resulting from conversion of molten pig iron to steel by oxidation of carbon impurities to harden the metal (Ishioka et al., 1992; Kim et al., 2016). These CO-rich by-product gases can be incinerated within the steel

45 production route for heat supply (Backes et al., 2021) or reused in the steelmaking process to replace some of the solid carbon fuels to reduce CO_2 emissions substantially (He and Wang, 2017; Kildahl et al., 2023). Understanding the CO loss processes throughout the entire steelmaking workflow and their link to CO_2 emissions is crucial for addressing the twin challenge of environmental pollution and climate change mitigation until the planned transformation to green steel is completed and the Blast Furnace–Basic Oxygen Furnace route has been replaced by the Direct Reduction–Electric Arc Furnace route using pure hy-

50 drogen (H_2) obtained from renewable sources as the reducing agent avoiding direct emissions of non-condensable greenhouse gases almost entirely (Graupner et al., 2023).

Given that the steel industry is highly energy-intensive and one of the leading industrial contributors to global anthropogenic CO_2 emissions, with a share of around 7%, the rapid and systematic decarbonisation of steel production is essential to meet climate targets (International Energy Agency, 2020). With around 40 million tonnes of crude steel production, Germany is the

55 largest steel producer in Europe and will likely exceed its sectoral CO_2 budget for a $1.5°C$ warming scenario in the 2030s at the latest (Harpprecht et al., 2022). In both Germany and worldwide, the predominant method accounting for around 70% of steel production is through primary production utilising the Blast Furnace–Basic Oxygen Furnace production route.

There are several studies analysing the environmental impact of steel production sites using a bottom-up life cycle assessment (Suer et al., 2022, and references therein), but most of them focus on CO_2 emissions and do not quantify co-emitted CO
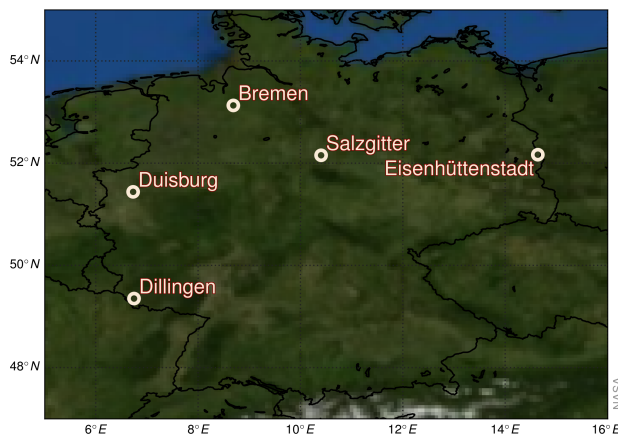
Figure 1. Locations of the analysed German steel production sites.

explicitly. One exception is the study by Burchart-Korol (2013), in which all inputs and outputs of the sub-processes involved in steelmaking are explicitly broken down for an integrated steel plant in Poland and summarised in a corresponding inventory. There are only a few studies on sector-specific CO emissions from steel production that were obtained by remote sensing. Atmospheric CO enhancements from steel production in Asia and Europe have been qualitatively analysed with TROPOMI data before (Schneising et al., 2019, 2023). Tian et al. (2022) quantify CO emission rates for industrial parks in Asia using TROPOMI data without attributing them to a specific sector. There are also some other analyses that deal with urban emissions (Park et al., 2021; Wu et al., 2022), but these are usually a mixture of emissions from different sectors, e.g. transport, heating, and industry-related. Wu et al. (2022) derive CO/CO_2 ratios for cities, including two in China that are explicitly highlighted as industry- and energy-oriented with metal production sites such as aluminium or steel plants.

In this manuscript, we use TROPOMI observations and their unique features to systematically quantify the CO emissions of all German steelworks applying the Linz–Donawitz process and to determine the corresponding sector-specific CO/CO_2 emission ratio, which is as a first step towards the potential use of co-emitted CO as a proxy for CO_2 emissions from the steel industry. The locations of the analysed production sites are shown in Figure 1.

2 Data and methods

Sentinel-5 Precursor, launched in October 2017, operates in a sun-synchronous orbit with an equator crossing time of 13:30 local time. TROPOMI is a spaceborne nadir-viewing imaging spectrometer designed to measure solar radiation reflected by the Earth in a push-broom configuration. With a swath width of $2600\,\mathrm{km}$, it provides a rare combination of relatively high spatial resolution and daily global coverage. The nadir measurements in the shortwave infrared (SWIR) offer a horizontal resolution of $5.5 \times 7\,\mathrm{km}^2$ at nadir ($7 \times 7\,\mathrm{km}^2$ before 6 August 2019) and are sensitive to all altitude levels, including the planetary boundary layer, making them well-suited for studying emissions from sources on the ground such as steelworks.
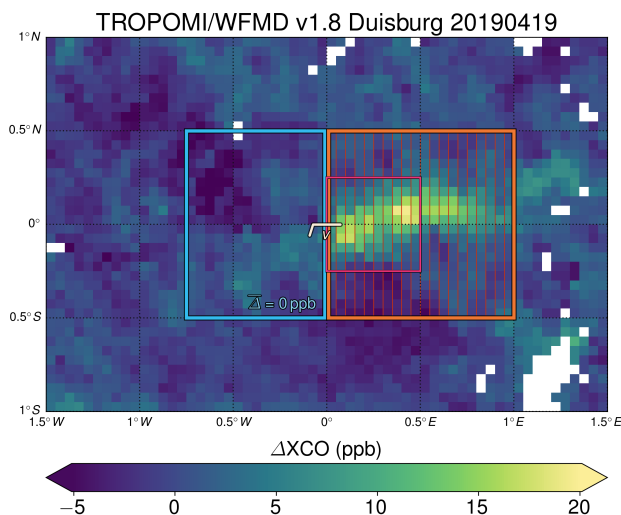
Figure 2. Example daily data for Duisburg to demonstrate the emission estimation process. The coordinate system has been rotated to the wind direction. The background region is highlighted in cyan, the plume region in orange, and the hot spot region in magenta. The dimensions and position of these regions remain constant for all days analysed within the rotated coordinate system. The hot spot region is only used to establish selection criteria that ensure sufficient data coverage (see main text for details) and is not used directly in the emission estimation process itself. The cross sections utilised for calculating the daily flux are indicated in red.

80 In this research, we use the latest version of the Weighting Function Modified DOAS (WFM-DOAS) algorithm, specifically optimised for the simultaneous retrieval of methane and carbon monoxide from TROPOMI (Schneising et al., 2019, 2023). The involved column-averaged dry air mole fractions of carbon monoxide, denoted as XCO, retrieved with the scientific TROPOMI/WFMD algorithm v1.8, are characterised by a random error (precision) of $5.1\,\mathrm{ppb}$ and a spatio-temporal systematic error (relative accuracy) of $2.6\,\mathrm{ppb}$ after quality filtering (Schneising et al., 2023).

85 The estimation of emissions presented here relies on the daily observations provided by TROPOMI and a Gaussian integral method, also referred to as the cross-sectional flux method. To automatically process quality-filtered daily XCO retrievals for a specific source region, the estimation method of Schneising et al. (2020b) is applied, which is briefly recapitulated in the following. Initially, the data given as latitude and longitude are transformed to a coordinate system rotated to the wind direction, in which the prime meridian and the equator are aligned with the centre of the analysed region and the zonal direction

90 corresponds to the mean boundary layer wind direction (within the region of interest and within a time window of two hours before the satellite overpass) obtained from the European Centre for Medium-Range Weather Forecasts (ECMWF) ERA5 reanalysis product (Hersbach et al., 2018). Subsequently, the transformed daily data is gridded on a $0.05° \times 0.05°$ grid, which is comparable to the horizontal nadir resolution of TROPOMI, and a mean background upwind of the source is subtracted. An example highlighting the position of the background and plume region is shown in Figure 2.

95 Let E represent the total column enhancement (in units of mass per area) and v the average wind speed within the boundary layer. To assess the emission, we use the divergence theorem and compute the flux of the vector field $E\boldsymbol{v}$ through cross

sections (red lines in Figure 2) perpendicular to wind direction, which is assumed to match the plume axis after rotation of the coordinate system. Consequently, the fluxes through boundaries other than the cross sections under consideration are zero, as the unit normals of the zonal boundaries are perpendicular to wind direction and there is no flux through any upwind meridional boundary. Thus, the emission rate is equal to the flux through the kth cross section for all k and given by

$$\Phi_k = \int_V (\boldsymbol{\nabla} \cdot E\boldsymbol{v})\, dV = \oint_{\partial V = S} E\boldsymbol{v} \cdot d\boldsymbol{S} = \sum_i E_{k,i}\, v\, \Delta l_i = v\, \Delta l \sum_i E_{k,i} = \frac{v \cdot \Delta l \cdot M_{CO} \cdot O_2}{N_A \cdot A_{CO} \cdot XO_2} \sum_i (\Delta XCO)_{k,i} \tag{1}$$

Here, Δl represents the size of a grid cell and i corresponds to the meridional summation along the respective cross section given by k. The molar mass of carbon monoxide, M_{CO}, is $28.01\,\mathrm{g\,mol^{-1}}$, the Avogadro constant, N_A, is $6.022 \cdot 10^{23}\,\mathrm{molec\,mol^{-1}}$, the O_2 column (in units of molecules per area) depends on the actual mean surface pressure, and the dry air mole fraction of oxygen, XO_2, is 0.209. These values are used to convert between the enhancement in XCO and the total column enhancement E. Additionally, A_{CO} is the value of the lowest layer of the averaging kernel (which is approximately 0.95 for all analysed source regions) characterising the boundary layer sensitivity of the retrieval method.

Taking the average of all cross-sectional fluxes Φ_k results in the daily flux estimate, denoted as Φ, with the corresponding uncertainty depending on the variability of the enhancements derived for the different cross sections, the variability of the absolute wind speed over the region, the wind history, and on the variability of the O_2 column, which is determined by surface pressure (Schneising et al., 2020b). In this daily averaging procedure, only those Φ_k are considered where at least 60% of the maximum possible grid cells along the cross-section are validly filled with data. If there are less than five such Φ_k, this particular day will not be used any further.

From the pool of available days, we select those that fulfill certain criteria (concerning data coverage, wind velocity, background scatter, meridional asymmetry, and wind history), which are listed below, for calculating the averaged long-term emission rate $\bar{\bar{\Phi}}$ of the respective source region (see Schneising et al. (2020b) for details). To better account for the quasi-point source character of steelworks in contrast to the larger emission regions analysed in Schneising et al. (2020b), we use smaller regions according to Figure 2 (e.g. cross sections of about $100\,\mathrm{km}$ length) and the following selection criteria optimised for XCO: at least 50% of the plume, hot spot, and background regions have to be filled with data (additionally at least 20% each of the northern and southern half of the background region), $v \in (1.5\,\mathrm{m\,s^{-1}}, 9\,\mathrm{m\,s^{-1}})$, the coverage and background distribution is required to be sufficiently uniform with respect to the equator ($n_p^N > 0.6 \cdot n_p^S$, $n_p^S > 0.6 \cdot n_p^N$, $|\bar{E}_b^N - \bar{E}_b^S| < 3\,\mathrm{ppb}$, $\sigma(E_b) < 4\,\mathrm{ppb}$), where $\bar{E}$ is the mean enhancement of a region, n is the corresponding number of grid cells, and σ is the standard deviation; $\cdot_{b,p}^{N,S}$ refers to the northern/southern half of the background/plume region. Additionally, days with wind direction changes exceeding $30°$ within the analysed wind history of 2 hours are also excluded. There is no criterion preventing negative meridional gradients ($\bar{E}_p < \bar{E}_b$) and associated negative emissions to ensure an unbiased mean long-term emission estimate $\bar{\bar{\Phi}}$. For small emissions, inversion noise can result in negative values, whose suppression would cause an overestimation of the mean emission. The calculation method for the uncertainty of the averaged long-term emission rate $\bar{\bar{\Phi}}$ from the individual daily uncertainties by error propagation has been retained exactly as described in Schneising et al. (2020b).

The European Union Emissions Trading System (EU ETS) regulates greenhouse gas emissions of energy-intensive industries and is based on the "cap and trade" principle. The cap limits the amount of greenhouse gases allowed to be emitted by an

installation and is quantified in emission allowances, which can be traded with each other. For each year, the companies operating the installations are obligated to surrender sufficient allowances to completely offset their actual emissions. Therefore, industrial installions are required to have an approved monitoring plan for monitoring and reporting annual emissions. These reported emissions data are verified annually by accredited independent verifiers (European Union, 2018). The corresponding

135 information is available on EUETS.INFO (https://www.euets.info/, last access: 14 November 2023) providing verified annual CO_2 emissions and surrendered allowances on the level of emitting installations and on country level.

The CO/CO_2 emission ratio is determined by Theil-Sen regression of the derived CO emissions for the different sites and the respective verified CO_2 emissions from the production of pig iron or steel available from the emission trading data. Theil-Sen regression is a robust method, which is insensitive to outliers and influential points by using the median of the slopes of all

140 possible lines formed by pairs of points (Sen, 1968). The corresponding confidence interval is determined by bootstrapping, fitting the Theil-Sen regressor to each resample, and analysing the resulting distribution of regression coefficients.

3 Results and discussion

The steel production sites in Germany that still utilise the conventional Blast Furnace–Basic Oxygen Furnace production route are located in Duisburg, Dillingen/Saar, Salzgitter, Bremen, and Eisenhüttenstadt (ordered by pig iron and steel production

145 from high to low), which together account for approximately 70% of German steel production (Harpprecht et al., 2022). These production sites have been analysed using the cross-sectional flux method to determine CO emissions during the time period 2018-2022.

3.1 Estimation of site-specific CO emissions

The North Rhine-Westphalian city of Duisburg has a long history as a centre of the steel industry as the region's proximity

150 to coal and iron ore reserves made it an ideal location for steel production. The city is home to two of the most prolific steel plants in Germany in service since more than a hundred years: Integriertes Hüttenwerk Duisburg with 4 blast furnaces and Glocke Duisburg with 2 blast furnaces. The averaged multi-year CO enhancement distribution for Duisburg, which exhibits a pronounced plume structure, and the daily emission estimates are displayed in Figure 3. The associated mean CO emission estimate is determined by the daily estimates and amounts to $397 \pm 58\,\mathrm{kt\,yr^{-1}}$.

155 The steel industry is one of the most important sectors of the economy in the German federal state of Saarland. Dillinger Hütte is the most significant steel producing site in the region, with production of steel dating back to the 17th century. Today, Dillingen is the only production site for pig iron in the Saarland, which is subsequently further refined into crude steel. Two blast furnaces are operated on the site. Figure 4 illustrates both the average CO enhancement distribution and the daily emission estimates for Dillingen. As in the case of Duisburg, there is a distinct plume shape visible in the long-term wind-rotated mean.

160 The corresponding mean CO emission estimate based on the daily emissions is $157 \pm 52\,\mathrm{kt\,yr^{-1}}$.

Salzgitter steel works is a Blast Furnace–Basic Oxygen Furnace steel plant operating in Salzgitter, Lower Saxony. The history of the site can be traced back to the interwar period in the early 20th century. During that time, an initiative aiming
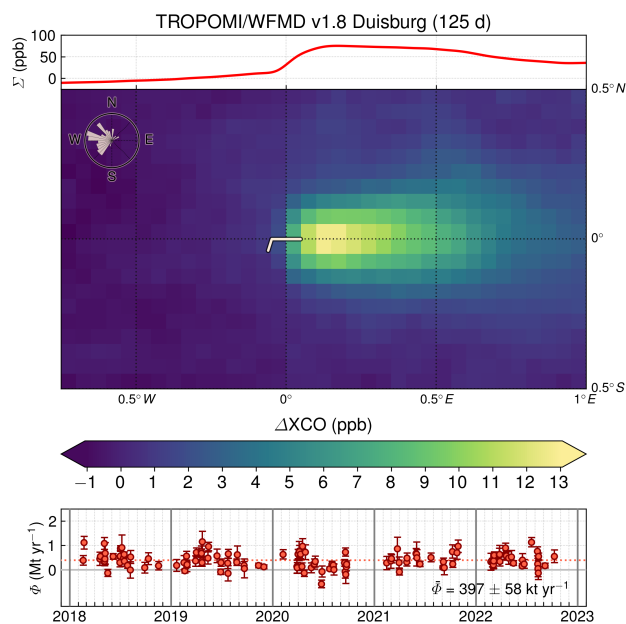
Figure 3. Mean CO enhancement distribution and associated integrated enhancement along the cross sections (top) as well as daily emission estimates Φ for the steel plants in Duisburg (bottom). The mean CO emission $\bar{\Phi}$ is calculated from the daily emissions. The original daily wind directions, defined as the direction in which the wind blows, are visually represented in the wind rose overlaid in the upper left corner.
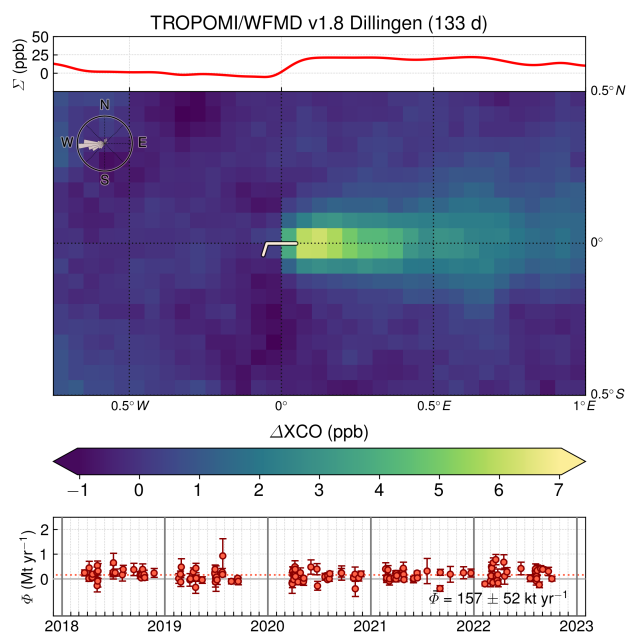
Figure 4. As Figure 3 but for Dillingen/Saar.
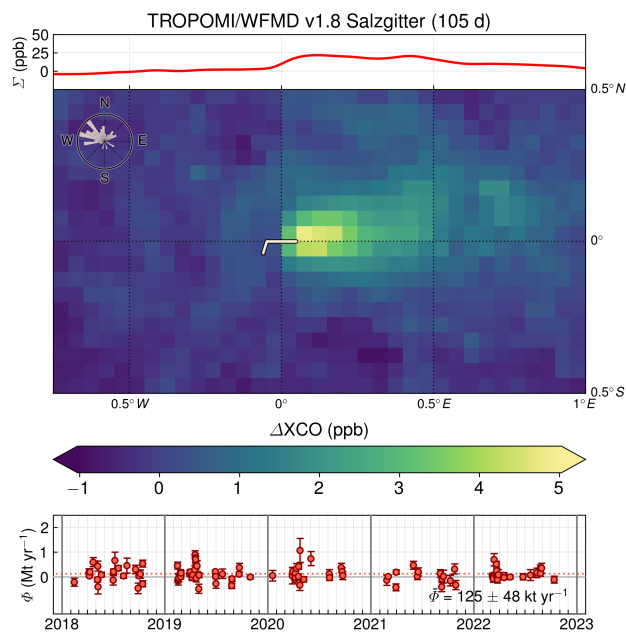
Figure 5. As previous figures but for Salzgitter.

at establishing a self-sufficient German steel industry included the construction of a massive steel plant in Salzgitter. After shutdown and recommissioning, the site operates 3 blast furnaces today. The mean CO enhancement distribution is shown
165   together with the daily emission estimates in Figure 5. The average CO emission is estimated to be $125 \pm 48\,\mathrm{kt\,yr^{-1}}$.

The Bremen steel plant with 2 blast furnaces has its roots in a long history of steel production in the region. The reason for establishing steelworks at this strategic location was the access to key transportation routes, including rivers and ports, that facilitated the import of raw materials and the export of finished steel products. Over the years, the plant underwent several redesigns, mergers and expansions to meet the changing needs of the steel industry. The averaged CO enhancement distribution
170   and the daily emission estimates are displayed in Figure 6. The associated mean CO emission estimate is $92 \pm 59\,\mathrm{kt\,yr^{-1}}$.

The history of the Eisenhüttenstadt plant located in the German federal state of Brandenburg began in the 1950s as the Eisenhüttenkombinat in East Germany producing pig iron with 6 blast furnaces. In the 1980s, a Linz–Donawitz steelworks was installed. After German reunification a new blast furnace was built, which is the only one still in operation today. Figure 7 illustrates both the average CO enhancement distribution and the daily emission estimates. The corresponding mean CO
175   emission estimate is $48 \pm 55\,\mathrm{kt\,yr^{-1}}$. In contrast to the other analysed production sites, the emissions seem to be close to the detection limit because only a rather weak plume is observable in the average CO distribution and there is hardly any variation of the associated sums along the cross-sections. In accordance with this finding, the mean emission estimate is similar in magnitude to the corresponding uncertainty indicating that the derived uncertainties are generally realistic.
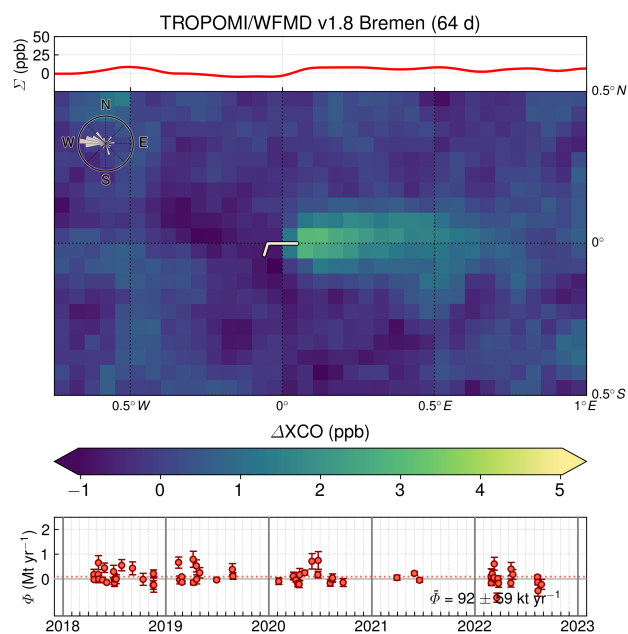
Figure 6. As previous figures but for Bremen.
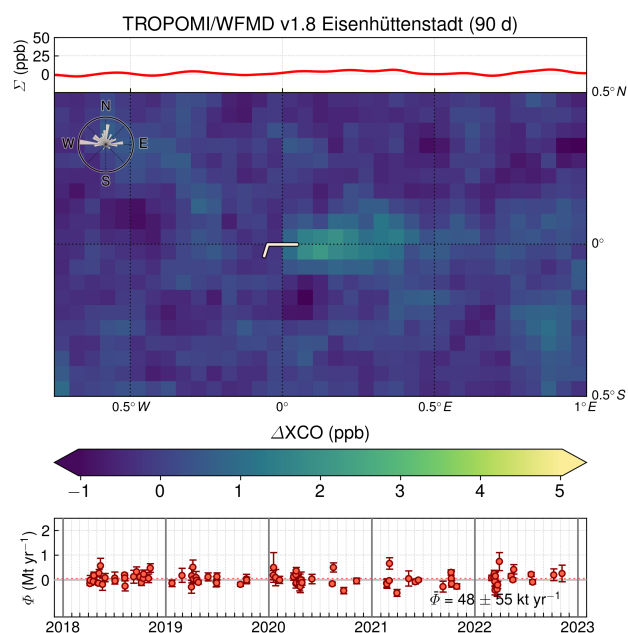
Figure 7. As previous figures but for Eisenhüttenstadt.

3.2 Air quality assessment

180 According to German air quality standards, the maximum allowed daily 8-hour mean of ambient CO is $10\,\mathrm{mg\,m^{-3}}$ (Umweltbundesamt, 2017). Typical background values in Germany are about $0.2\,\mathrm{mg\,m^{-3}}$ (Umweltbundesamt, 2022). The largest local daily enhancement anomalies occurring in the vicinity of German steelworks reach about $50\,\mathrm{ppb}$ in very rare cases, which translate to a total column enhancement E of roughly $0.5\,\mathrm{g\,m^{-2}}$. It is assumed that the excess CO from the steel production site is located in the well-mixed boundary layer and that the associated boundary layer concentration anomaly $\Delta\rho_{bl}$ (in units

185 of mass per volume) can be determined by division by the boundary layer height h_{bl} (Schneising et al., 2020a):

$$\Delta\rho_{bl} = \frac{E}{h_{bl}} \tag{2}$$

Assuming a boundary layer height of $500\,\mathrm{m}$, the boundary layer anomaly is about $1\,\mathrm{mg\,m^{-3}}$, which is well below the air quality standard of $10\,\mathrm{mg\,m^{-3}}$ even after adding typical background concentrations.

The figures in Section 3.1 show that the maximum annual averaged enhancements due to steelworks are of the order of

190 $10\,\mathrm{ppb}$ locally, which corresponds to an annual mean boundary layer anomaly of about $0.2\,\mathrm{mg\,m^{-3}}$ using the above assumptions. Adding a typical background value gives a maximum total annual mean concentration at TROPOMI resolution of about $0.4\,\mathrm{mg\,m^{-3}}$ in the vicinity of steel production sites, which is in agreement with actually measured values, e.g. in Dillingen (Umweltbundesamt, 2022). Consequently, the rough calculation has confirmed that the CO emissions from the analysed steelworks are not an air quality issue.

195 ## 3.3 Sector-specific CO/CO$_2$ emission ratio

The European Union Emissions Trading System (EU ETS) provides verified annual CO_2 emissions on the level of emitting installations. The associated mean emissions of the steel production sites for the time period analysed here (2018-2022) are summarised in Table 1.

Figure 8 demonstrates that CO and CO_2 emissions from the production of pig iron or steel are highly correlated. It is

200 assumed that the temporal sampling of available daily CO emission estimates is representative for the actual variability of steel production and associated reported CO_2 emissions at the analysed sites. As the data point representing Duisburg is quite far away from the main cluster of data points, it may be an influential point with large impact on the results when performing an ordinary least-squares (OLS) regression, which potentially complicates the interpretation of the fitted coefficients and their uncertainties. This potential issue can be mitigated by using the robust Theil-Sen regression (Sen, 1968), which calculates the

205 slope by taking the median of all possible slopes between individual pairs of data points. To compute a confidence interval for the Theil-Sen regression, we use bootstrapping (plus additional random perturbation of the data points in y-direction according to the respective uncertainties of the individual CO emission estimates) to generate multiple resamples of the data and fit the Theil-Sen Regressor to each resample. This results in a set of regression coefficients from which the final regression and the associated 1σ-confidence interval are derived by determining the median of slopes and intercepts as well as the 16th and 84th

210 percentile of the distribution.

Table 1. Mean emissions for the time period 2018-2022. The CO_2 emissions from the production of pig iron or steel are obtained from the European Union Emissions Trading System (EU ETS), the CO emissions are estimated in this study as well as extracted from the Thru.de portal (providing key environmental data from industrial facilities in Germany) for comparison.

Site	ID	Operator	Blast furnaces	EU ETS CO_2 emissions (Mt yr^{-1})	This study CO emissions (kt yr^{-1})	Thru.de CO emissions (kt yr^{-1})
Duisburg	DU	Thyssenkrupp Steel Europe	4	7.75	397 ± 58	315
		Hüttenwerke Krupp Mannesmann	2	4.61		
Dillingen	DI	Dillinger Hüttenwerke	2	4.15	157 ± 52	90
Salzgitter	SZ	Salzgitter Flachstahl	3	3.92	125 ± 48	66
Bremen	HB	ArcelorMittal Bremen	2	2.30	92 ± 59	63
Eisenhüttenstadt	EH	ArcelorMittal Eisenhüttenstadt	1	1.48	48 ± 55	40
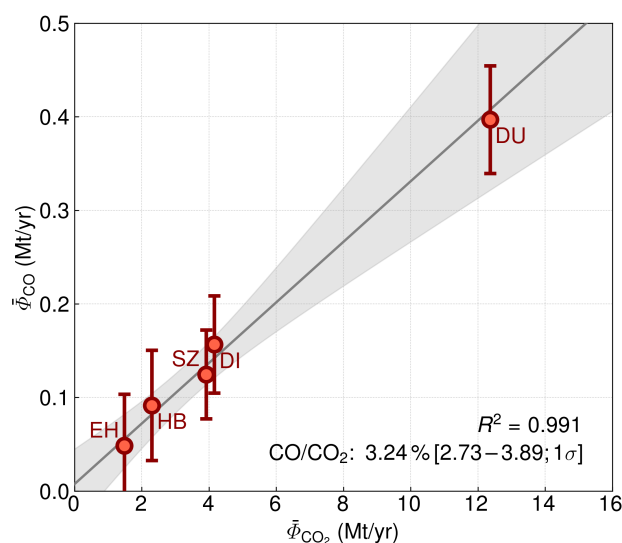
Figure 8. Theil-Sen regression of the derived CO emissions for the different sites and the respective CO_2 emissions according to the European Union Emissions Trading System (EU ETS) to determine the CO/CO_2 emission ratio and the associated 1σ-confidence interval. The shaded region surrounding the regression line represents the prediction interval, which is determined by assessing the standard deviation of Theil-Sen regressions from multiple bootstrap samples. R^2 is the coefficient of determination of the prediction of the Theil-Sen regression.

The performed robust Theil-Sen regression of CO and CO_2 emissions is illustrated in Figure 8. The shaded area around the regression line visually represents the prediction interval, which is determined by the standard deviation of the regressions of the multiple bootstrap samples and effectively reflects the predictive uncertainty of the model. The resulting CO/CO_2 emission

ratio for the analysed steelworks amounts to $3.24\%\,[2.73-3.89;\,1\sigma]$; the corresponding 95%-confidence interval (obtained from
215 the 2.5th an 97.5th percentile of the slope distribution) is $[1.90, 5.50]$.

This sector-specific estimate can be hardly compared to global inventories such as the Emissions Database for Global Atmospheric Research (EDGAR) (Crippa et al., 2020) because the underlying sector discrimination is typically not detailed enough. For example, iron and steel production is part of the EDGAR activity "Industrial combustion and processes" that also includes sectors with significantly less CO emissions than steelworks at comparable CO_2 emissions. Consequently, the EDGAR
220 CO/CO_2 emission ratio for the entirety of industrial processes is smaller than our sector-specific estimate for the steel industry and amounts to about 0.5% for Germany. Similar representativeness issues arise when comparing to the estimated CO/CO_2 ratios for cities of Wu et al. (2022): their estimate for the Chinese cities with metal production is about 1% (when transformed to a mass ratio) but there are also other sectors, such as energy production, with significantly smaller CO/CO_2 emission ratios (significant CO_2 emissions, but virtually no CO emissions) contributing to the derived city averages.

225 Another register of emissions from industrial facilities in Germany is the Thru.de portal provided by the Umweltbundesamt (https://thru.de/en/, last access: 14 November 2023) including annual loads of CO and CO_2 based on measurements, calculations, or estimates of the operators. The reported values are reviewed for completeness and plausibility by authorities at federal state level, but unlike the emissions trading data used to derive the CO/CO_2 emission ratio, no independent verification is required. Using the reported Thru.de mean releases from the German metal industry for the years 2018-2022, the associated
230 CO/CO_2 emission ratio is approximately 2.0%. However, this value cannot be directly compared with ours either, because this activity also comprises other processes than conventional primary steel production. Deriving a sector-specific emission ratio based on Thru.de data is also not straightforward because the reported releases are not provided on the level of emitting installations (in contrast to the European Union Emissions Trading System), but on the facility level. A facility is defined as one or more installations at the same site that are run by one operator. For example, a facility in the steel industry (integrated
235 steelworks) may include a large number of different installations (e.g. coking plant, sintering plant, blast furnace, basic oxygen furnace, rolling mill, power plant), whose combined emissions are then attributed to the so-called *main activity* of the facility, which is usually the production of pig iron or steel. While the CO emissions are actually mainly attributable to the main activity, the reported CO_2 emissions typically also include significant contributions from other sectors such as the energy sector. As a consequence, the facility-based Thru.de CO/CO_2 emission ratio underestimates the actually targeted sector-specific emission
240 ratio, just like the other potential comparison data sets discussed so far. However, the extent of underestimation is not even consistent from site to site, but depends on which non-main activities are explicitly carried out additionally at a given facility. It is therefore not possible to obtain a representative CO/CO_2 emission ratio from this data set by regressing the individual CO and CO_2 emissions of the respective facilities. Nevertheless, the reported Thru.de CO releases can be directly compared with our emission estimates, because only the place of origin and not the exact breakdown by sector is relevant for this pur-
245 pose. The corresponding values are also listed in Table 1. In general, the reported Thru.de CO releases are systematically smaller than our estimates. If the respective uncertainties are taken into account, there is no significant deviation in Bremen and Eisenhüttenstadt, but systematic residual underestimates of less than 20% in the Thru.de data at the other sites.

The estimate that is conceptually closest to our estimate is obtained by using the outputs of the sintering plant, blast furnace, and basic oxygen furnace of the comprehensive inventory of a Polish integrated steel plant (Burchart-Korol, 2013) resulting in
250   a CO/CO_2 emission ratio of 2.60%. This value is considerably closer to our sector-specific estimate for steel production than the other less representative estimates and within the associated 95%-confidence interval (even near the estimated 1σ-range). This consistency further corroborates the potential feasibility of using CO as a proxy for CO_2 emissions from comparable steel production sites.

4   Conclusions

255   We conducted an analysis of carbon monoxide enhancements originating from German steel plants using the conventional highly CO_2-intensive Blast Furnace–Basic Oxygen Furnace production route. This analysis utilised daily measurements in the shortwave infrared spectral range of the TROPOMI instrument on board the Sentinel-5 Precursor satellite to estimate the CO emissions for these steelworks during the 2018-2022 period benefiting from TROPOMI's distinctive attributes, including its high quality measurements and comprehensive spatio-temporal coverage. These qualities enable us to systematically detect
260   and quantify sufficiently large emission sources during a single satellite overpass.

Together with the comprehensive availability of verified site-specific CO_2 emission data from the production of pig iron or steel available from the European Union Emissions Trading System, an estimate for the associated sector-specific CO/CO_2 emission ratio is derived. The high correlation of CO and CO_2 emissions suggests that the raw material use and the involved processes are comparable and reproducible for the steelworks studied. The focus on German steel plants has the advantage that
265   the accurate reporting of CO_2 emissions within the framework of emissions trading enables a good calibration of the CO/CO_2 emission ratio, which is thus of significant value to use CO as proxy for CO_2 emissions from the steel industry in particular for comparable Linz–Donawitz steel plants, also in less regulated countries with less stringent reporting requirements.

If locally observed CO emissions are very sector-specific, i.e. the vast majority of CO emissions can be attributed to a single sector, as in the case of pig iron or steel production analysed here, the usage of realistic installation-based bottom-up CO_2
270   emission data broken down by activity type simplifies obtaining sector-specific CO/CO_2 emission ratios. In contrast, this is difficult to achieve by means of space-based CO_2 measurements, because emissions from the sector in question are potentially entangled with atmospheric signals from nearby anthropogenic CO_2 emissions associated with other sectors such as electricity production, as well as natural sources and sinks. Future accurate CO_2 satellite missions with very high spatial resolution could help to better separate emissions from neighbouring anthropogenic sources belonging to different sectors from space.

275   *Data availability.* The carbon monoxide data product presented in this publication is available at http://www.iup.uni-bremen.de/carbon_ghg/ products/tropomi_wfmd/.

Author contributions. OS designed and operated the TROPOMI/WFMD satellite retrievals, performed the data analysis, interpreted the results, and wrote the paper. MB, MR, MW, HeB, JPB, HB made significant contributions to the conception of the analysis and the improvement of the manuscript. All authors discussed the results and commented on the paper.

280 *Competing interests.* The authors declare that they have no conflict of interest.

Acknowledgements. This publication contains modified Copernicus Sentinel data (2018-2022). Sentinel-5 Precursor is an ESA mission implemented on behalf of the European Commission. The TROPOMI payload is a joint development by ESA and the Netherlands Space Office (NSO). The Sentinel-5 Precursor ground-segment development has been funded by ESA and with national contributions from The Netherlands, Germany, and Belgium. We thank the European Centre for Medium-Range Weather Forecasts (ECMWF) for providing the
285 ERA5 reanalysis and acknowledge the use of carbon dioxide emission data from the European Union Emissions Trading System (EU ETS) (https://www.euets.info/, last access: 14 November 2023).

Financial support. The research leading to the presented results received funding from the European Space Agency (ESA) via the projects GHG-CCI+ and MethaneCAMP (ESA contract nos. 4000126450/19/I-NB and 4000137895/22/I-AG) and from the German ministry of education and research (BMBF) within its project ITMS via grant 01 LK2103A. The TROPOMI/WFMD retrievals presented here were
290 performed on HPC facilities of the IUP, University of Bremen, funded under DFG/FUGG grant nos. INST 144/379-1 and INST 144/493-1. The article processing charges for this open-access publication were covered by the University of Bremen.

References

Backes, J. G., Suer, J., Pauliks, N., Neugebauer, S., and Traverso, M.: Life Cycle Assessment of an Integrated Steel Mill Using Primary Manufacturing Data: Actual Environmental Profile, Sustainability, 13, https://doi.org/10.3390/su13063443, 2021.

295 Bovensmann, H., Burrows, J. P., Buchwitz, M., Frerick, J., Noël, S., Rozanov, V. V., Chance, K. V., and Goede, A. P. H.: SCIAMACHY – Mission Objectives and Measurement Modes, J. Atmos. Sci., 56, 127–150, https://doi.org/10.1175/1520-0469(1999)056<0127:SMOAMM>2.0.CO;2, 1999.

Burchart-Korol, D.: Life cycle assessment of steel production in Poland: a case study, Journal of Cleaner Production, 54, 235–243, https://doi.org/10.1016/j.jclepro.2013.04.031, 2013.

300 Burrows, J. P., Hölzle, E., Goede, A. P. H., Visser, H., and Fricke, W.: SCIAMACHY – Scanning Imaging Absorption Spectrometer for Atmospheric Chartography, Acta Astronautica, 35, 445–451, https://doi.org/10.1016/0094-5765(94)00278-T, 1995.

Crippa, M., Solazzo, E., Huang, G., Guizzardi, D., Koffi, E., Muntean, M., Schieberle, C., Friedrich, R., and Janssens-Maenhout, G.: High resolution temporal profiles in the Emissions Database for Global Atmospheric Research, Scientific Data, 7, 121, https://doi.org/10.1038/s41597-020-0462-2, 2020.

305 Drummond, J. R., Zou, J., Nichitiu, F., Kar, J., Deschambaut, R., and Hackett, J.: A review of 9-year performance and operation of the MOPITT instrument, Adv. Space Res., 45, 760–774, https://doi.org/10.1016/j.asr.2009.11.019, 2010.

European Union: Commission Implementing Regulation (EU) 2018/2067 of 19 December 2018 on the verification of data and on the accreditation of verifiers pursuant to Directive 2003/87/EC of the European Parliament and of the Council, available at: http://data.europa.eu/eli/reg_impl/2018/2067/2021-01-01 (last access: 6 November 2023), 2018.

310 Graupner, Y., Weckenborg, C., and Spengler, T. S.: Low-carbon primary steelmaking using direct reduction and electric arc furnaces: Prospective environmental impact assessment, Procedia CIRP, 116, 696–701, https://doi.org/10.1016/j.procir.2023.02.117, 30th CIRP Life Cycle Engineering Conference, 2023.

Harpprecht, C., Naegler, T., Steubing, B., Tukker, A., and Simon, S.: Decarbonization scenarios for the iron and steel industry in context of a sectoral carbon budget: Germany as a case study, Journal of Cleaner Production, 380, 134 846,
315 https://doi.org/10.1016/j.jclepro.2022.134846, 2022.

He, K. and Wang, L.: A review of energy use and energy-efficient technologies for the iron and steel industry, Renewable and Sustainable Energy Reviews, 70, 1022–1039, https://doi.org/10.1016/j.rser.2016.12.007, 2017.

Hersbach, H., de Rosnay, P., Bell, B., Schepers, D., Simmons, A., Soci, C., Abdalla, S., Alonso-Balmaseda, M., Balsamo, G., Bechtold, P., Berrisford, P., Bidlot, J.-R., de Boisséson, E., Bonavita, M., Browne, P., Buizza, R., Dahlgren, P., Dee, D., Dragani, R., Diamantakis, M.,
320 Flemming, J., Forbes, R., Geer, A. J., Haiden, T., Hólm, E., Haimberger, L., Hogan, R., Horányi, A., Janiskova, M., Laloyaux, P., Lopez, P., Munoz-Sabater, J., Peubey, C., Radu, R., Richardson, D., Thépaut, J.-N., Vitart, F., Yang, X., Zsótér, E., and Zuo, H.: Operational global reanalysis: progress, future directions and synergies with NWP, ERA Report Series, https://doi.org/10.21957/tkic6g3wm, 2018.

Holloway, T., Levy II, H., and Kasibhatla, P.: Global distribution of carbon monoxide, Journal of Geophysical Research: Atmospheres, 105, 12 123–12 147, https://doi.org/10.1029/1999JD901173, 2000.

325 International Energy Agency: Iron and Steel Technology Roadmap: Towards more sustainable steelmaking, available at: https://www.iea.org/reports/iron-and-steel-technology-roadmap (last access: 14 November 2023), 2020.

Ishioka, M., Okada, T., and Matsubara, K.: Formation and characteristics of vapor grown carbon fibers prepared in Linz-Donawitz converter gas, Carbon, 30, 975–979, https://doi.org/10.1016/0008-6223(92)90124-F, 1992.

Kildahl, H., Wang, L., Tong, L., and Ding, Y.: Cost effective decarbonisation of blast furnace – basic oxygen furnace steel production through thermochemical sector coupling, Journal of Cleaner Production, 389, 135 963, https://doi.org/10.1016/j.jclepro.2023.135963, 2023.

Kim, T. W., Bae, S. S., Lee, J. W., Lee, S.-M., Lee, J.-H., Lee, H. S., and Kang, S. G.: A biological process effective for the conversion of CO-containing industrial waste gas to acetate, Bioresource Technology, 211, 792–796, https://doi.org/10.1016/j.biortech.2016.04.038, 2016.

MacDonald, C. G., Mastrogiacomo, J.-P., Laughner, J. L., Hedelius, J. K., Nassar, R., and Wunch, D.: Estimating enhancement ratios of nitrogen dioxide, carbon monoxide and carbon dioxide using satellite observations, Atmos. Chem. Phys., 23, 3493–3516, https://doi.org/10.5194/acp-23-3493-2023, 2023.

Park, H., Jeong, S., Park, H., Labzovskii, L. D., and Bowman, K. W.: An assessment of emission characteristics of Northern Hemisphere cities using spaceborne observations of CO2, CO, and NO2, Remote Sensing of Environment, 254, 112 246, https://doi.org/10.1016/j.rse.2020.112246, 2021.

Schneising, O., Buchwitz, M., Reuter, M., Bovensmann, H., Burrows, J. P., Borsdorff, T., Deutscher, N. M., Feist, D. G., Griffith, D. W. T., Hase, F., Hermans, C., Iraci, L. T., Kivi, R., Landgraf, J., Morino, I., Notholt, J., Petri, C., Pollard, D. F., Roche, S., Shiomi, K., Strong, K., Sussmann, R., Velazco, V. A., Warneke, T., and Wunch, D.: A scientific algorithm to simultaneously retrieve carbon monoxide and methane from TROPOMI onboard Sentinel-5 Precursor, Atmos. Meas. Tech., 12, 6771–6802, https://doi.org/10.5194/amt-12-6771-2019, 2019.

Schneising, O., Buchwitz, M., Reuter, M., Bovensmann, H., and Burrows, J. P.: Severe Californian wildfires in November 2018 observed from space: the carbon monoxide perspective, Atmos. Chem. Phys., 20, 3317–3332, https://doi.org/10.5194/acp-20-3317-2020, 2020a.

Schneising, O., Buchwitz, M., Reuter, M., Vanselow, S., Bovensmann, H., and Burrows, J. P.: Remote sensing of methane leakage from natural gas and petroleum systems revisited, Atmos. Chem. Phys., 20, 9169–9182, https://doi.org/10.5194/acp-20-9169-2020, 2020b.

Schneising, O., Buchwitz, M., Hachmeister, J., Vanselow, S., Reuter, M., Buschmann, M., Bovensmann, H., and Burrows, J. P.: Advances in retrieving XCH$_4$ and XCO from Sentinel-5 Precursor: improvements in the scientific TROPOMI/WFMD algorithm, Atmos. Meas. Tech., 16, 669–694, https://doi.org/10.5194/amt-16-669-2023, 2023.

Sen, P. K.: Estimates of the Regression Coefficient Based on Kendall's Tau, Journal of the American Statistical Association, 63, 1379–1389, 1968.

Suer, J., Traverso, M., and Jäger, N.: Review of Life Cycle Assessments for Steel and Environmental Analysis of Future Steel Production Scenarios, Sustainability, 14, https://doi.org/10.3390/su142114131, 2022.

Suto, H., Kataoka, F., Kikuchi, N., Knuteson, R. O., Butz, A., Haun, M., Buijs, H., Shiomi, K., Imai, H., and Kuze, A.: Thermal and near-infrared sensor for carbon observation Fourier transform spectrometer-2 (TANSO-FTS-2) on the Greenhouse gases Observing SATellite-2 (GOSAT-2) during its first year in orbit, Atmos. Meas. Tech., 14, 2013–2039, https://doi.org/10.5194/amt-14-2013-2021, 2021.

Tian, Y., Sun, Y., Borsdorff, T., Liu, C., Liu, T., Zhu, Y., Yin, H., and Landgraf, J.: Quantifying CO emission rates of industrial point sources from Tropospheric Monitoring Instrument observations, Environmental Research Letters, 17, 014057, https://doi.org/10.1088/1748-9326/ac3b1a, 2022.

Umweltbundesamt: Informationen zum Luftschadstoff Kohlenmonoxid (CO), available at: https://www.umweltbundesamt.de/sites/default/files/medien/370/dokumente/infoblatt_kohlenmonoxid_0.pdf (last access: 14 November 2023), 2017.

Umweltbundesamt: Air data: Annual tabulation (CO), available at: https://www.umweltbundesamt.de/en/data/air/air-data/annual-tabulation/eJxrWpScv9BoUWXqEiMDIyMAMLgFtA== (last access: 14 November 2023), 2022.

Veefkind, J. P., Aben, I., McMullan, K., Förster, H., de Vries, J., Otter, G., Claas, J., Eskes, H. J., de Haan, J. F., Kleipool, Q., van Weele, M., Hasekamp, O., Hoogeveen, R., Landgraf, J., Snel, R., Tol, P., Ingmann, P., Voors, R., Kruizinga, B., Vink, R., Visser, H., and Levelt, P. F.: TROPOMI on the ESA Sentinel-5 Precursor: A GMES mission for global observations of the atmospheric composition for climate, air quality and ozone layer applications, Remote Sensing of Environment, 120, 70–83, https://doi.org/10.1016/j.rse.2011.09.027, 2012.

370 Wu, D., Liu, J., Wennberg, P. O., Palmer, P. I., Nelson, R. R., Kiel, M., and Eldering, A.: Towards sector-based attribution using intra-city variations in satellite-based emission ratios between CO_2 and CO, Atmos. Chem. Phys., 22, 14 547–14 570, https://doi.org/10.5194/acp-22-14547-2022, 2022.